

## **Optimizing the Patient's Dose in Dental Ortho-Pantomographic X-ray by a Bayesian Approach, Utilizing the Scatter-Glare Prior Probability calculated by Monte Carlo Simulations**

Peter Michael Goebel<sup>1,2,3</sup>, Ahmed Nabil Belbachir<sup>1</sup>, Michael Truppe<sup>3</sup>

<sup>1</sup> *Vienna University of Technology, Institute of Computer Aided Automation, PRIP, Favoritenstrasse 9/1832, Vienna, Austria 1040, <[goe.nabil@prip.tuwien.ac.at](mailto:goe.nabil@prip.tuwien.ac.at)>*

<sup>2</sup> *University of Applied Science, fh-campus-wien, Technical Project- and Process-Management, TPPM, Eitenreichgasse 45a, Vienna, Austria 1100*

<sup>3</sup> *Karl Landsteiner Institute for Biotelematics, Danube University Krems, Austria 3500 [mtruppe@landsteiner.org](mailto:mtruppe@landsteiner.org)*

### **ABSTRACT**

The reduction of the x-ray dose that offers higher safety for the patient reduces diagnostic image quality. Recently, we have shown appropriate methods for the auto computation of the noise-estimate [1] and for the reconstruction [2] of dental panoramic images. The noise-estimate is calculated by a semi-empirical scatter-glare model of the photon projection-process and a wavelet based method for the subtraction of the energy of the noise-estimate from the energy of the panoramic image. The analysis of the reconstruction results stemming from the processing of a database of 50 ortho-pantomographic images shows excellent improvement of contrast and detectability of diagnostic detail at reduced noise level.

In this paper, the modeling of the semi-empirical scatter-glare model for the photon projection-process by Monte Carlo calculations is explained in more detail, and an improved Bayesian calculation of the posterior scatter-estimate is presented.

### **INTRODUCTION**

In recent years panoramic radiography developed to one of the major complementary examinations in dentistry. However, dental radiographs are taken periodically and more often than any radiographs. A fact that coincides with higher public awareness of the risks associated with the exposure to ionizing radiation. New objectives on lowering dental caries, periodontal diseases and tooth loss, are currently devised by the World Health Organization for the year 2020 Oral Health Program. To minimize the impact of oral and craniofacial diseases on health and psychosocial development of individuals, the 2020 Oral Health Program is arguing for early diagnosis and prevention.

Even though the dosage of radiation is small compared to other types of radiographs, some people are still inflicted by dental anxieties, fears, and phobias against x-ray examinations. Therefore, lowering the dose, as well as providing sufficient information, regarding the procedure, are effective strategies to overcome the aforementioned obstacles. As a consequence of increased safety for patients, the quality of the resulting images degrades substantially, thus such images may suffer from relevance. Enhancement of relevant details and suppression of unwanted artifacts, such as noise and

other distortions, is the aim of reconstruction methods, which try to meet these contradictory requirements.

In this paper a semi-empirical model for the generation of a spatially adaptive noise map is implemented under some simplifying conditions, which is cross checked with data from the NIST database [3] and Monte Carlo simulations by the GEANT4 simulation package. The projection scattering process at the atomic level is subdivided into a prior calculation part and a posterior one. The prior part generates a table of scatter priors, which is then used for the posterior calculation of a spatial noise variance map for an actual diagnostic image. As the noise contribution in the diagnostic image stems from scattered photons, which still survives all scattering events, the traveling paths of such photons are altered, thus, they are detected at random locations, resulting in scatter-glare fog. The removal of that scatter-glare fog enables an appropriate contrast enhancement.

#### **STATE OF THE ART**

Statistical models for images are described in [S97], whereas in [PS03] the application of Gaussian scale mixtures (GSM) to natural images is given. The estimation of noise itself is left open by many authors. A comparative study between six methods is shown in [O93]. A method for blind estimation of noise variance is given in [MJR90] and the references herein.

Adaptation to unknown noise variance by a locally adaptive Wiener Filter was done by Lee [L80] using the spatial image domain. When the Lee filter is applied to a region that contains signal activity (i.e. lines and edges), the filter reduces its smoothing characteristic, whereas in regions with constant intensity it responds with its initial smoothing characteristic. Thus, the filter has smoothing properties in that regions, while still preserving sharp details. The drawbacks are that it cannot detect weak detail and it leaves noise in the vicinity of edges and lines.

Most approaches suppose the noise is of Gaussian nature; some suppose a Poisson distribution or a combination of both distributions. An overview of wavelet methods in medical image processing is given by Unser [UAL03]. Mallat [M89] founded by his work "A theory for multiresolution signal decomposition: The wavelet representation" the basic approach to obtain the discrete wavelet transform (DWT) from multiresolution analysis.

In their seminal work Donoho and Johnstone [DJ94], considered "ideal adaption via wavelet shrinkage" (i.e. VisuShrink), where for a  $N \times N$  image an universal threshold was proposed. The method truly removes the noise, but the image content is oversmoothed. In "the adaption to unknown smoothness" Donoho and Johnstone [DJ95] defined "SureShrink", which is thresholding by applying level adaptive thresholds, a separate threshold is computed for each detail subband based upon SURE (Stein's unbiased estimator for risk), which applies to probable coefficients of noise the universal threshold of VisuShrink. Although the method exhibits good mathematical convergence, the visual results are not convincing.

Vidakovic [V98] uses Bayesian methods to model the relevant properties of the DWT coefficients with prior probability distributions. Upon obtaining the likelihood function from a noise model the resulting (i.e. the posterior) distribution can be calculated from a sample distribution (i.e. the prior). Specifying a loss function yields estimation rules pursuant to the Bayesian decision theoretic approach. Figueiredo [FN01]

generalized the process of how signals can be manipulated by applying the DWT. Processing consists in manipulating the DWT coefficients, rather than the signal samples themselves, in three steps: (1) Computation of the DWT coefficients of the signal, (2) Performing some specified processing on the coefficients, and (3) Computation of the inverse DWT to obtain the resulting signal.

In general, wavelet methods utilize that three steps and most of them differ only in the second processing step. In Goebel and Brändle [BG03] the application of filtering by coefficient shrinkage in the Fourier- and Wavelet-domain was investigated. It was shown that a Wiener filter applied directly to the wavelet coefficients yields better results in terms of preservation of sharp details, but the images were contaminated by artifacts. Brown [JB00] proposed an adaptive enhancement algorithm that uses the correlation between wavelet coefficients, at the same spatial position in successive resolution levels, in order to discriminate between coefficients arising from noise and those arising from signal features. Browns work was successful on mammograms to find micro calcifications in breast tissue for cancer prevention, but applied to DPR it changed the overall look of the radiographs, which was not acceptable from the view of the physicians.

Nowak and Baraniuk [NB99] proposed a method of wavelet-domain filtering for photon imaging systems assuming Poisson statistics and cross validation by using N low photon count images to design an optimal wavelet-domain filter. Whereas the method is a common practice for astronomical image acquisition, the method can be used only for direct digital radiographic systems, because of the required high number N of detailed images. Naimuddin Shaikh [S89] proposed to use a convolution algorithm for estimation of scatter and glare in diagnostic radiology and have used a look-up table utilizing scatter-glare back-projection within the noise estimation model.

Single parts of the proposed methods did already exist; however, the way of combining them, extending and filling gaps by means of new concepts appears to be new. From that point of view the following works are closely related to and are basics concepts to the proposed approach of this thesis, although the concepts are adapted to the purpose. The simulation of x-ray scattering, using the same parameters as used for the real imaging process, enables to produce a forward projection estimate for the photon scatter. That estimate can be used, by a back projection process, for the generation of a noise image estimate. Plancherel's Theorem ensures the conservation of energy if images are transformed to/from the multiresolution domain. Therefore, the noise image estimate can be subtracted from the original x-ray image to enable better image quality (without or with lesser noise contribution). As a fact, the achieved better image quality paves the way to reduce the photon rate during an x-ray imaging process, which lowers the dose for the patient.

#### **PROBLEM DEFINITION**

The research question of the herein proposed approach aims in: *"finding a solution to achieve high diagnostic image quality in concurrence to the reduction of the radiographic dose."* This paper proposes an answer to that research question by assessing basic requirements; and generating a solution by merging the research fields of physics, medicine, statistics, and image processing in a multidisciplinary manner.



Figure 1: A comparison of the effects caused by lowering the radiographic dose. The left image shows an ordinary standard radio graph stemming from a human dummy head and the right image shows the same, but with lowered dose. One can see the degradation caused in the right image compared to the left one.

Figure 1.1 shows twice the same region of a radio graph of a human dummy head, but one (at the left) for a normal filtration, and one (at the right) for additional filtration to lower the dose. Even, the image values are scaled contrast for printing, the image at the right is more degraded by noise, since the signal to noise ratio (SNR) is lowered. The effects that mostly contribute to the deterioration (degradation) of image quality and the corresponding issues are identified as:

1. The systematic non-homogeneous illumination (NHIL) from the x-ray source: the photon rate is increased to permeate the spine region during a panoramic scan, which causes a multiplicative influence on the image values.
2. The contrast adaptation of the human visual system (HVS) to the level of background illumination: the psychophysical detection of differences in contrast (i.e. detection thresholds) by the human eye is modulated in a nonlinear way by the intensity of the background.
3. The impact of scatter noise (SCN) statistics: the true image statistics are still rather inconclusive; inappropriate noise filtering may degrade the image furthermore.

### **The De-noising Problem**

Common methods to eliminate contributions of noise are deconvolution techniques, applied in the context of linear or non-linear filtering. Classical filtering, designed for the suppression of high frequencies, prove as inadequate as they fail to preserve information regarding details. Adaptive filters (e.g. Wiener Filter) have problems to distinguish between noise variance and variance from the informative image content.

Among others, the most popular method for image denoising is multiscale filtering, based on the wavelet transform. The basic idea is to decompose an image according to different frequency bands and at different scales, by a non-decimating multiresolution transform, resulting in an over complete (i.e. redundant) translation invariant representation of the transformed space. The deterministic image content is represented by a set of a few stronger coefficients, whereas the noise is distributed across all coefficients at weak intensity.

To illustrate the problem, in Figure 2, a classical denoising approach is performed by wavelet coefficients thresholding using a usual noise variance estimate.

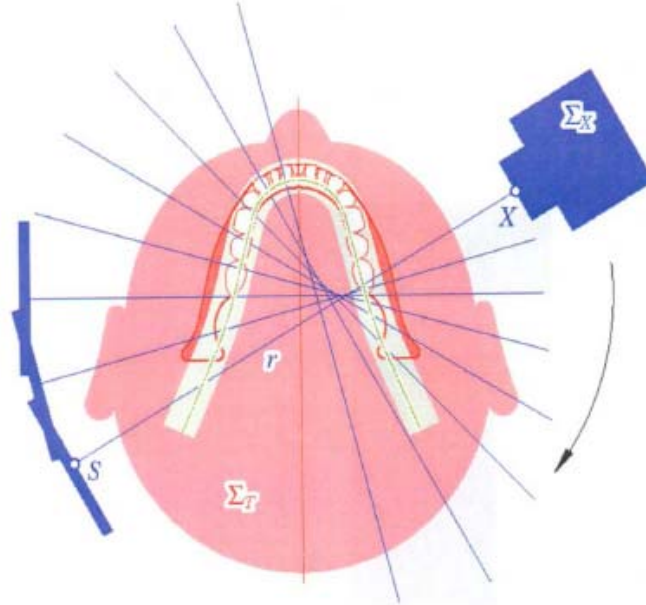


Figure 2: Comparison of effects for classical denoising: A high resolution CT image, as a reference (shown by the left image), shows the ideal view for a diagnostic image with a high level of detail; Gaussian and Poisson noise is added to the CT image (shown by the middle image), details are still observable; From the classically denoised version of the CT image with added noise (shown by the right image), one can see a typical blurring effect of the edge information.

A classical denoising approach is performed by wavelet coefficients thresholding using a usual noise variance estimate [DJ94]. Consequently, Figure 2 rightmost image shows the majority of noise being eliminated, while the resulting image is blurred. Within the weak wavelet coefficients there is hidden edge information, therefore fine details in the image are lost.

### **Panoramic Projection Radiography**

A main tool in dental radiography is the x-ray projection image that reveals the inner structure of bone and teeth. Dental Panoramic Radiography DPR is a technique where the entire dentition is projected onto a sensing device.



**Figure 3: Principle Schema of a Dental Panoramic Radiography DPR System.  $\Sigma_x$  represents the x-ray generator; X the x-ray beam; r the beam; and S the sensor.**

In principle, there are three types of sensing devices: direct or indirect x-ray films; photostimulable storage phosphor (PSP) plates; and solid state semiconductor sensor arrays. Source and detector are in opposition, rotating around the patients head. The focal area of the x-ray beam describes a planar curve, which is standardized for the human teeth and jaw. The photon rate is increased near the jaw center to permeate the spine region, during a panoramic scan, symmetrically, which causes a multiplicative influence on the image values. From the primary poly-energetic x-ray beam, photons are absorbed (i.e. scattered) along the path between source and detector by the patients matter (muscle, fat, bone, air, or contrast agents). The photon attenuation of each type of matter depends on its elementary and chemical composition as well as on the beam. Image degradation is caused by defected primary photons due to scattering events, which still reach the sensor, resulting in scatter-glare fog.

## THE NEW SEMI-EMPIRICAL MODELLING APPROACH

The authors have recently shown in [8] that the noise statistics of dental OPT images follow a mixture of two generalized Gamma distributions, rather than pure Poisson distributions, where one of them stems from photon attenuation scatter (i.e. the absorbed photons) and the other from the photon scatter-glare (i.e. photons whose traveling paths have changed, and have not been absorbed), which is accountable to the noise contribution.

### Deriving the Image Model by Blind Source Separation (BSS)

The principally ill posed, since inverse<sup>1</sup>, process of BSS in general is the separation of a set of  $n$  statistically independent signals  $s = [s_1 \dots s_n]$  from a set of  $m$  observed signals  $x = [x_1 \dots x_m]$ , tied together by a mixing matrix  $\mathbf{A}$ , leading to a solution  $x = \mathbf{A}s$ . This yields a solution, where the image is treated as a mixture from (at least two) independent sources, a photon source  $I_0$  that is attenuated by matters, and a background  $B$ . During a diagnostic radiological investigation the attenuation by the patient matter is of interest, but the aggregation of all sources together of no-interest is classified as the background  $B$ . We are interested in the pure diagnostic information, which we are not able to measure directly, since it is contaminated by the background equivocation. The BSS idea starts with observations that can be made objectively by the equipment. Thus we get the linear equation system

$$\begin{pmatrix} I_1 \\ I_2 \end{pmatrix} = \mathbf{A} \begin{pmatrix} I_0 \\ B \end{pmatrix}$$

with  $I_1$  and  $I_2$  as two independent observations (i.e.  $I_1$  is an image taken without phantom/patient, thus it is the background illumination image;  $I_2$  is the actual diagnostic image of the phantom/patient) from an experimental setup, using a known phantom;  $I_0$  is the unobservable output intensity of the x-ray tube; and  $\mathbf{A}$  is the mixing matrix, determined by the experimental setup. Evaluating the linear equation system and treating

---

<sup>1</sup> We call two problems inverses of one another if the formulation of each involves all or part of the solution of the other. Often, for historical reasons, one of the two problems has been studied extensively for some time, while the other has never been studied and is not so well understood. In such cases, the former is called the direct-problem, while the latter is the inverse-problem (Keller, 1976). The linear inverse problem yields a discrete linear algebraic system, which may provide a mathematical solution. For example, the information loss due to an imaging filtering process cannot be derived from the remaining data. Therefore, some additional information is needed, namely a priori or prior information. Such a problem is called well-posed, when its solution is unique, exists for arbitrary data and is continuous. A small variation in the data should not cause a considerably variation in the solution. The crux of the difficulty is that even if a mathematically tractable solution exists, however, it may happen that it is not acceptable from a physical point of view. Consequently, the problems that are not well-posed are called ill-posed, incorrectly posed or improperly posed.

all variables, except mixing matrix  $\mathbf{A}$  as random vectors; and utilizing the expectation of the random vectors, because the digitized images are in fact the result from an expectation operation, yields

$$\begin{aligned} E\{I_1\} &= \underbrace{a_{11}E\{I_0\}}_{\text{filtration data}} + a_{12}E\{B\} \\ E\{I_2\} &= \underbrace{a_{21}E\{I_0\}}_{\text{filtration+patient data}} + a_{22}E\{B\} \end{aligned}$$

with  $E\{\cdot\}$  symbolizing the expectation<sup>2</sup> operator; and  $I_0$  is estimated by a Monte-Carlo simulation of the energy spectrum of the x-ray generator, accordingly to the actual acquisition parameters used. The calculation of the patient's absorption (ABS) data yields

$$E\{\tilde{I}_2\} = E\{I_1\} - E\{I_2\} + E\{B\}(a_{22} - a_{12})$$

with  $\tilde{I}_2$  the reconstructed diagnostic image. The result indicates the need for an appropriate estimate for the background  $B$ , scaled by the factor  $(a_{22} - a_{12})$  derived from the (i.e. ill-posed) transformation matrix  $\mathbf{A}$ . The background  $B$  is then classified by exerting a multiplicative behavior of the elements of matrix  $\mathbf{A}$  on the photon load  $I_0$ , with its expectation  $E\{I_0\}$  is varying accordingly to the systematical intensity modulation regarding the compensation of the contrast loss caused by the spine bone density and the non-linear influence by scatter noise. Unfortunately, due to the high nonlinearity of the matrix coefficients', this form of the background estimate is mathematically intractable. Therefore, one can derive another solution in introducing the transmittance  $T$

$$T = \frac{I_2}{I_1} = \frac{a_{21}I_0 + a_{22}B}{a_{11}I_0 + a_{12}B}$$

if one assumes the informative content of  $I_1$  as informative only as its informative content is at low frequencies only, and taking the expectation from  $E\{I_1\}$  by a median to remove the background, in the denominator, yielding

$$\frac{I_2}{\hat{I}_1} = \frac{a_{21}I_0 + a_{22}B}{a_{11}I_0} = \underbrace{\frac{a_{21}}{a_{11}}}_{\text{transmittance}} + \underbrace{\frac{a_{22}B}{a_{11}I_0}}_{\text{noise contribution}}$$

The last term is that of noise, which can be exploited by the application of a Gaussian scale mixture model (GSM). A GSM is a model of a mixture of independent infinite Gaussians, scaled by a hidden scale factor  $\xi$  to the variance value of evidence, thus yields

$$\left(\frac{I_2}{\hat{I}_1}\right) = T + \xi(x, y, \sigma^2) N(0, 1)$$

---

<sup>2</sup> The expectation operator is defined as  $E\{X\} = \int_{-\infty}^{+\infty} xf(x)dx$  with  $X$  is a random variable, defined on its probability space

with  $T$  symbolizing the noise free transmittance image,  $\xi$  is the scale factor,  $x$  and  $y$  are pixel coordinates, and  $N(0; 1)$  is locally Gaussian noise with mean zero and a variance equating to one. Thus, subtracting that field of random will properly reconstruct the transmittance image  $T$ . Therefore, for eliminating the impact of noise in the diagnostic image applying an additive noise model will suffice if an artificial, spatial adaptive noise estimate for the original noise can be generated. To ensure statistical independence from the original image, the noise estimate will be exploited from a physically convenient simulation of photon-scattering at the atomic level by a semi empirical Bayesian model, where the prior-distribution is calculated offline for the entire diagnostic energy range (i.e. for instant use). The posterior-distribution is then calculated by using maximum likelihoods (ML) generated from an actual diagnostic image and a background image, yielding a coherent factor noise map, which is used to generate the artificial noise estimate as an infinite realization of an infinite mixture of Gaussian distributions (i.e. a Gaussian Scale Mixture).

### Scatter Event Likelihood Decomposition by Monte Carlo Simulation

Panoramic x-ray systems are using poly-energetic x-ray, thus the absorption coefficients by scattering are highly nonlinear and are depending on the photon energy (see Figure 1). For the estimation of the scatter-glare noise contribution, the knowledge of the scatter interaction is crucial. X-ray photons from the source with Poisson statistics are absorbed along the path between the source and detector by the patient's matter (muscle, fat, bone and air or contrast agents; see Figure 2).

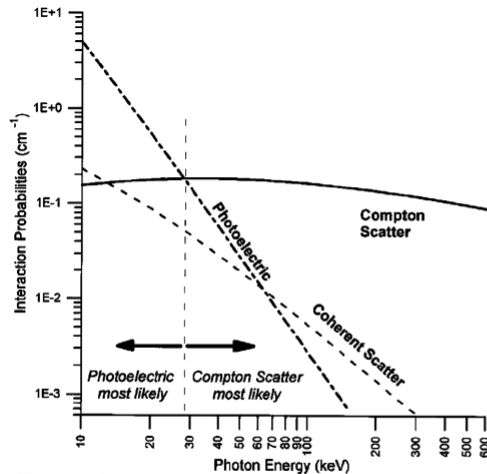


Figure 1: Relationship of Interaction Probabilities for Coherent-, Photoelectric- and Compton Scatter to Photon Energy [13].

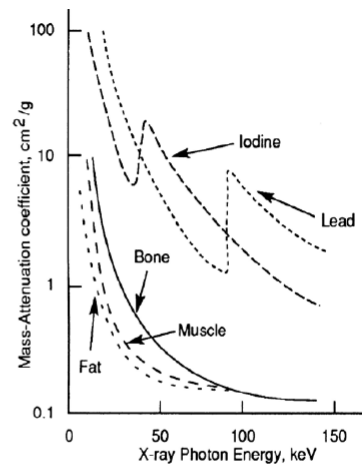


Figure 2: Non-linear Relationship between Photon Energy and Mass Attenuation for Various Tissue [10].

The scattering of the photons, by photoelectric, Compton and coherent interactions<sup>3</sup>, causes two effects due to their crossing of matter: firstly, an attenuation of the photon beam by a different type or thickness of matter (that excites the generation of the radiographic image); secondly, surviving scattered photons darken the film while carrying no useful information, because their path is randomly altered, resulting in scatter-glare noise.

Here again, we encounter an ill-posed problem, because during the forward projection, the scatter events sum up in the detector, and the resulting projection image represents the scattering likelihood<sup>4</sup>, since all of the information in all occurred scatter events is contained in that likelihood function. Thus, in an actual diagnostic image, the likelihoods are known from the pixel values, but nothing about their spectral composition. Therefore, a decomposition approximation method is developed by the simulation of an x-ray projection process.

Utilizing the GEANT4 framework, starting with the predefined "PhotonProcesses" from the GEANT4 extended example section, and defining two setups for the geometrics of an aluminum step-wedge and a PMMA flat phantom, generates a table of scatter-glare likelihoods – i.e. simulated images of the step-wedge and the PMMA phantoms. The scatter events from the photoelectric, Compton and coherent interactions are recorded prior to its summation in the Detector. A type of look-up table is generated that can make a projection in forward direction – that is the summation of the three scatter events – and can be used also for a back projection – that is the recall of the recorded scatter event triplet for a desired likelihood (i.e. a image pixel value).

An alternate model, utilizing the TASIMP software as x-ray generator and an approximate implementation of the scatter characteristics accordingly to Figure 1 is implemented in MatLab (Mathworks Inc.) and the following modeling parameters:

- a) *Coherent scatter is modeled as Rayleigh scatter only:  $\sigma_{\text{coh}} = 1/\sqrt[5]{E^6}$*
- b) *Compton scatter is assumed to be constant in [10..100keV]:  $\sigma_{\text{incoh}} = 0.15$*
- c) *For both cases, a) and b), scatter is assumed to be independent of Z*
- d) *The photoelectric scatter  $\tau$  is assumed to vary accordingly to:  $\tau = Z^4/E^3$ .*

with E is the photon energy, Z is the effective atomic number. The result of that model, compared to the NIST data base give a good performance in the restricted energy range for diagnostic panorama images. Figure 3 shows a comparison between the scatter event probabilities achieved by the simplified model and data from the NIST database.

---

<sup>3</sup> Diagnostic energy range 5..100keV

<sup>4</sup> Likelihood is the hypothetical probability that an event that has already occurred would yield a specific outcome. The concept differs from that of a probability in that a probability refers to the occurrence of future events, while likelihood refers to past events with known outcomes. It is the conditional distribution P(B|A) of B given the data A.

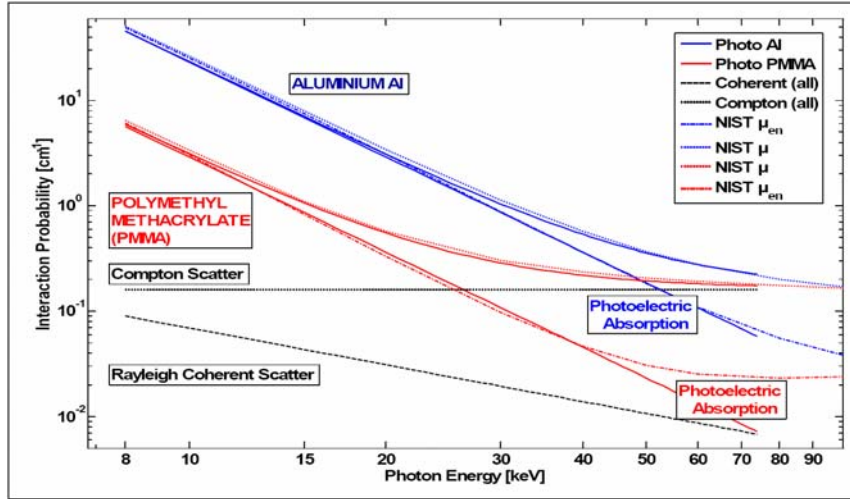


Figure 3: The simplified Probabilistic Photon Scatter Model. The total scattering by the exploited model, for aluminum and PMMA, is related to the NIST database. Photoelectric scatter is shown in blue for aluminum for  $\mu$  and  $\mu_{en}$  (the energy transfer coefficients), and in red both for PMMA.

In Figure 3, the total scattering for aluminum and PMMA in terms of the linear attenuation coefficient  $\mu$  applied as

$$\mu = \tau + \sigma_{incoh} + \sigma_{coh}$$

is related to scattering data from the NIST database [SH95] (dotted lines). Up to 40keV the energy transfer coefficients  $\mu_{en}$  are also in good relation to the photoelectric absorption. Above that point, the model has an upcoming divergence, especially for softer matters (i.e. PMMA), but their interaction probability is quite low, thus the error may be neglected for the proposed application in medical imaging.

### Estimating the Spatially Adaptive Noise Map

Figure 4 shows an overview of the developed estimator, which is a composition of a prior calculation part and a posterior one. The prior part generates a table of scatter priors, which is then used for the posterior calculation of a spatial noise variance map for an actual diagnostic image.

The x-ray energy spectrum  $E$ , generated by the TASIMP simulation program [BS97] is available as a table of normalized photon flux, which is parameterized to include the geometrical situation, the exposure time, the milliamperage and the maximum energy (1). The forward projection (2) results in a table of pixel values (3), and also in the corresponding table of scatter priors (4). The look-up table realizes the backward projection. In the context of Bayesian probability theory and statistical inference, its alternate form may be exploited for the calculation of distributions

$$f_{post}(x|y) = \frac{f_{like}(y|x) \times f_{prio}(x)}{f_{norm}(y)}$$

with  $f_{post}(x|y)$  is the posterior distribution of  $X$  given  $Y$ ;  $f_{like}(y/x)$  is the likelihood function of  $X$  given  $Y$ ;  $f_{prio}(x)$  is the prior distribution of  $X$ ; and  $f_{norm}(y)$  is the marginal distribution of  $Y$ . The table of scatter priors (4) contains the results of the scatter-estimates for each possible likelihood value (i.e. pixel). The background estimate (5) together with actual pixel values (6) and the scatter-priors (4) calculates the scatter-glare amount in (7) by

$$pdf_{post}(x|y) = \frac{pdf_{scatter-glare}(x)}{pdf_{scatter}(y)} \times pdf_{like}$$

As the result, an adaptive spatial map of the diagnostic noise variance is produced. The map is used to generate the noise estimate by scaling the variance of a random Gaussian noise field with zero mean and variance one  $N(0; 1)$ .

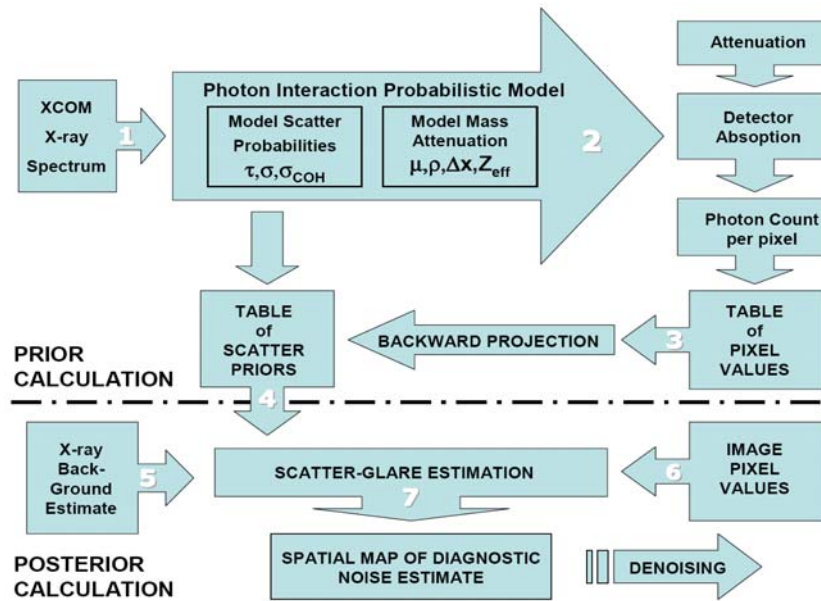


Figure 4: The Scatter Estimation Model has two main parts: the upper one is the prior part for the calculation of a scatter prior table. Module1 generates the x-ray energy spectrum by using the TASIMP simulation program, which is part of XCOM. The photon interactions are implemented in Module2, and the simulation of the detector yields the table of pixel values as Module3. The outcome of the prior calculation is the table of scatter priors in Module4. The lower part of the model is dedicated to the posterior processing. A background image as Module5; an actual image as Module6 and the scatter-prior table (i.e. Module4) are used to form an estimate of the scatter glare in Module7. The estimate of the scatter glare forms the spatial noise estimate.

In particular, in the denoising approach, the noise function is modeled by the Nakagami distribution. Stressing Plancherel's Theorem, the energy of the noise estimate is then subtracted from the noisy transmittance image in the wavelet domain (see Fig. 5). The reconstructed estimate of the transmittance provides reduced noise contribution by preserving diagnostic detail. The result of the noise estimation approach was used by

Goebel et. al. in [7] for OPT image restoration. The approach was tested against classical wavelet hard- and soft-thresholding methods. It was shown that it performed substantially better than the former in terms of modulation transfer function (MTF) and signal to noise ratio (SNR).

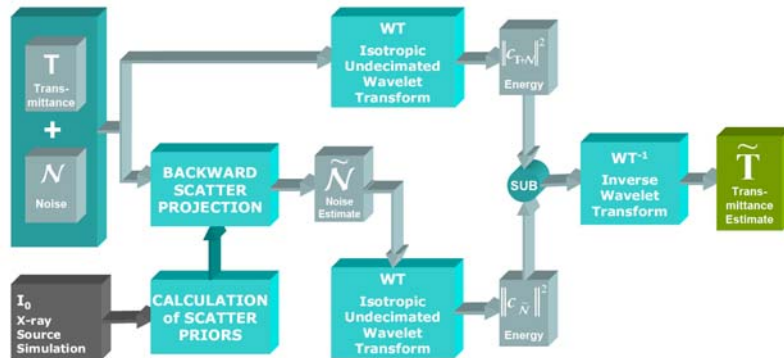


Figure 5: The subtraction of the noise estimate from the diagnostic image mixture by utilizing the conservation of energy within the wavelet space. The model exploits an empirical Bayesian approach for the auto-calculation of the backward scatter projection.

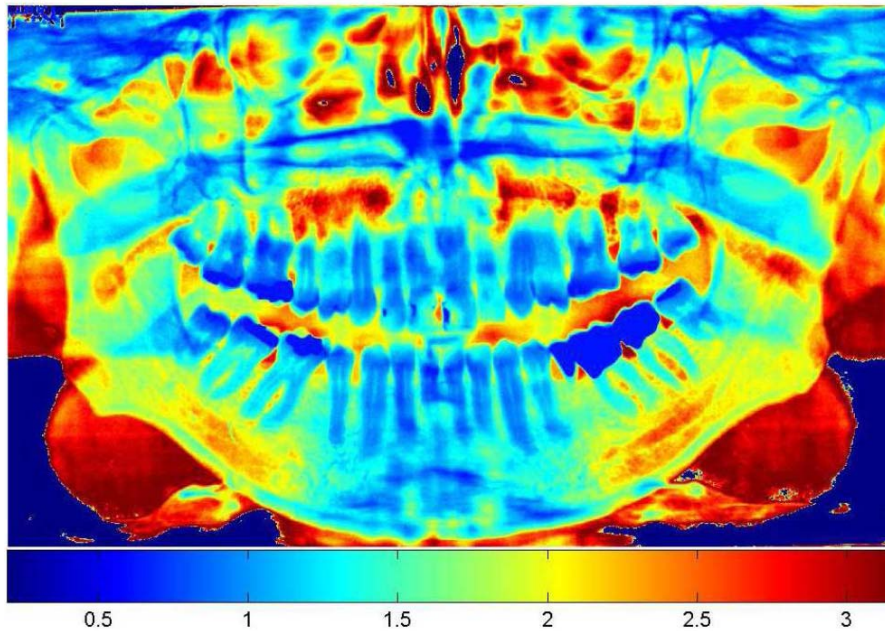


Figure 6: A dedicated noise coherence factor  $x(x; y)$  image. In the areas of interest, the factors are below 1, which causes softer denoising.

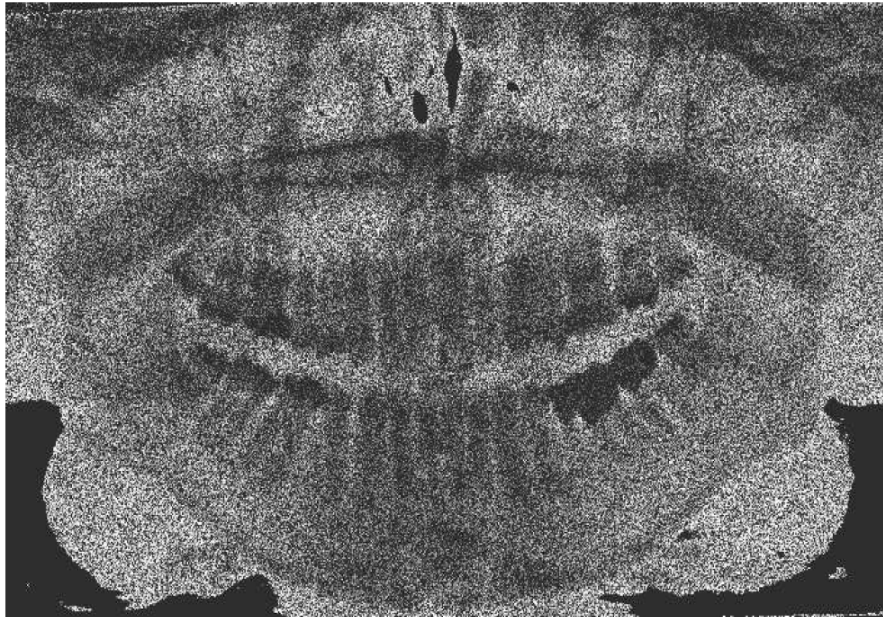


Figure 7: The noise estimate to Figure 6

After the posterior is calculated, using the likelihood and the prior. The result is a coherence map (see Figure 6), which reflects the dependence of the noise on the actual diagnostic image content. In the coherence map, the scatter-glare is estimated, which forms the rule that specifies how much denoising is applied to the mixture image. In Figure 6 a factor below one specifies less denoising, which is accomplished inside the teeth, while a factor greater than one forces stronger denoising in the areas between the teeth. From the coherence map a Gaussian scale mixture (GSM) is exploited, where the coherence factors calculates up for the hidden scale factor  $\xi(x; y)$ . That  $\xi(x; y)$  scales a Gaussian noise image field with predefined noise  $N(0; 1)$  {zero mean, variance one} and forms the noise estimate in Figure 7. The noise estimate of Figure 4.11 is subtracted by (3.9) in the multiresolution domain from the mixture image, after the multiresolution reconstruction.

#### **The Relative Dose Assessment**

There is no simplistic approach to determine the radiographic dose, because of the nonlinear behavior between polyenergetic x-ray beam and photon attenuation. Therefore, in this section, an experimental assessment is presented. For the assessment of the absorbed dose the comparison of the imparted intensity of a human dummy head phantom is used. The assessment is a relative assessment how much the radiographic dose is lowered by taking two consecutive radiographs from the fixated phantom with and without the 6 mm aluminum filter. The human dummy head is masked to prevent from including stray radiation. The linear dose reduction factor is calculated by the fraction of integral of the imparted intensities, which means that the additional aluminum

probably reduces the radiographic dose by a factor of about 2:2 at x-ray parameters 73kVp and Milliamperage 15 mA.

### **CONCLUSION**

A procedure for estimation of the noise in panoramic x-ray images, where the local statistics are calculated from a database of 50 images. A noise model was created, with the main purpose to achieve optimal image quality after denoising. The noise model supports the separation of the information of interest by ideas stemming from Blind Source Separation. The method opens the possibility for reduced patient dose, because of the good reconstruction properties of the approach of this thesis. The image degradation by the reduced photon count could be compensated, furthermore it was shown that it is possible to remove the noise contribution and concurrently keep the diagnostic information. Blurring effects, known from other methods are only minor perceivable.